



PHOTONICS Research

Electric tuning of plasmonic resonances in ultrathin gold nanoribbon arrays

ZHENXIN WANG,¹ ALEXEY V. KRASAVIN,² CHENXINYU PAN,¹ JUNSHENG ZHENG,¹ ZHIYONG LI,^{1,3}  XIN GUO,^{1,3} ANATOLY V. ZAYATS,² LIMIN TONG,¹ AND PAN WANG^{1,3,*} 

¹State Key Laboratory of Extreme Photonics and Instrumentation, College of Optical Science and Engineering, Zhejiang University, Hangzhou 310027, China

²Department of Physics and London Centre for Nanotechnology, King's College London, Strand, London WC2R 2LS, UK

³Jiaying Key Laboratory of Photonic Sensing & Intelligent Imaging, Intelligent Optics & Photonics Research Center, Jiaying Research Institute Zhejiang University, Jiaying 314000, China

*Corresponding author: nanopan@zju.edu.cn

Received 28 March 2024; revised 16 May 2024; accepted 27 May 2024; posted 29 May 2024 (Doc. ID 522533); published 1 August 2024

Ultrathin plasmonic nanostructures offer an unparalleled opportunity for the study of light–matter interactions at the nanoscale and realization of compact nanophotonic devices. In this study, we introduce an ultrathin gold nanoribbon array and demonstrate an electric approach to actively tuning its plasmonic resonance, which leveraging the extreme light confinement capability in the ultrathin plasmonic nanostructure and a robust nanoscale electro-optical effect in indium tin oxide. Optimizing the design (to a total thickness as small as 12 nm for a 2-nm-thick gold nanoribbon array), we numerically demonstrate a spectral shift in the plasmonic resonance up to 36 nm along with an approximately 16% change in the transmission at a gate voltage below 1.7 V at the wavelength of 1.47 μm . This work presents progress towards electric tuning of plasmonic resonances in ultrathin metallic nanostructures for various applications including surface-enhanced spectroscopy, spontaneous emission enhancement, and optical modulation. © 2024 Chinese Laser Press

<https://doi.org/10.1364/PRJ.522533>

1. INTRODUCTION

Surface plasmons in metallic nanostructures have continuously attracted extensive research attention because of their ability to break the diffraction limit and confine electromagnetic fields at the subwavelength scale that can greatly enhance light–matter interaction [1,2]. This has triggered a series of breakthroughs in fundamental nanophotonic studies [3–7] together with the realization of highly compact nanophotonic devices, such as (bio)chemical sensors, nano-lasers, optical modulators, and photodetectors [8–18]. Recently, ultrathin (few nanometers in thickness) noble-metal films have sparked great research interest because they can support extremely confined plasmonic modes in the visible and near-infrared (vis-NIR) spectral regions, and provide an enhanced nonlinear optical response [19–26]. This is further driven by the development in fabrication technologies for high-quality ultrathin gold and silver films [21,22,26–28]. Combined with the advanced nanofabrication technology, these ultrathin noble-metal films can be patterned into ultrathin plasmonic structures [21,25,26], which allow access to the regime of extreme light–matter interactions for fundamental studies, as well as the development of applications such as surface-enhanced spectroscopy, spontaneous emission enhancement, high-sensitivity optical sensing, and optical modulation.

While the near- and far-field response of ultrathin plasmonic structures can be tailored by engineering the geometrical parameters, it is highly desired to have the ability to tune it dynamically [29]. On one hand, this is necessary for shifting the plasmonic resonance, which is highly sensitive to fabrication errors for ultrathin metallic nanostructures [26], to the designed wavelength; on the other hand, development of a dynamically tunable plasmonic resonance can enable an on-demand enhancement of light–matter interactions, which can remarkably extend the scope and applicability of ultrathin plasmonic nanostructures for applications such as surface-enhanced spectroscopy [12,30], spontaneous emission enhancement [31,32], and light modulation [33–36]. Among the various tuning approaches (e.g., based on thermal, electrochemical, mechanical, electrical, and optical mechanisms) [15,37–41] developed for metallic nanostructures, electric tuning is of great interest because of its advantages including fast response time and easy integration. Indium tin oxide (ITO), as a highly efficient electro-optical material, has been widely used for electric tuning of plasmonic response in metallic nanostructures [35,36,42–45]. However, due to the ultrathin thickness (few-nanometer scale) of the electrically induced accumulation layer (i.e., the active region with an electrically induced permittivity change), it is mostly exploited for electric tuning of

metal–insulator–metal or metal–insulator–semiconductor plasmonic structures, in which a strong overlap between the plasmonic modes and the nanometer scale accumulation layer in ITO can be achieved.

Here, by combining the extreme light confinement capability in ultrathin plasmonic nanostructures with the efficient nanoscale electro-optical effect in ITO, we propose an all-solid-state electric approach to efficiently modulate plasmonic resonances in ultrathin gold nanoribbon arrays. We demonstrate that an ultrathin thickness of the gold nanoribbons, enabled by a recently developed fabrication technology, plays a crucial role in the efficiency of electric tuning of the plasmonic response. Exploiting the above advantages, we numerically show that a spectral shift in the plasmonic resonance up to 36 nm along with a 16% change in the intensity of the transmission dip of a 2-nm-thick gold nanoribbon array can be realized with an application of gate voltage below 1.7 V. These results open a new avenue towards the electric tuning of plasmonic resonances in ultrathin gold nanostructures and may find applications in miniaturized devices for surface-enhanced spectroscopy, spontaneous emission enhancement, and signal processing.

2. DESIGN AND PRINCIPLE OF OPERATION

Recent developments in ultrathin monocrystalline gold films [26,46,47] with low loss and strong field localization allow for development of new nanophotonic designs. In this work, ultrathin gold nanoribbon arrays (GNRAs, nanoribbons in the array are not coupled with a period three times the nanoribbon width), which support ultraconfined dipolar plasmonic resonances and can be readily fabricated in a large scale [21,22,26], were exploited for the electric tuning investigation. Figure 1 shows a schematic illustration of the proposed design for electric tuning of plasmonic resonance in an ultrathin GNRA, which is embedded in a high- k dielectric, hafnium oxide (HfO_2) and then sandwiched between two ITO layers. When normally incident light having polarization perpendicular to the nanoribbons illuminates the array, it excites nanoribbon dipolar plasmonic resonances, which results in a dip in the spectral dependence of the transmission. When a positive voltage is applied between the GNRA and the ITO layers (upper panel of Fig. 1), a nanoscale electron accumulation layer is induced in the ITO at the ITO/ HfO_2 interfaces [48], which leads to the modulation of the refractive index of the ITO in this region, including both real and imaginary (absorptive) parts. As the plasmonic resonance is highly localized around the nanoribbons and the thickness of HfO_2 is just a few nanometers [35], there is a good overlap between the mode electromagnetic field and the region of the refractive index change in the ITO, which makes the plasmonic resonance of the GNRA very sensitive to the induced refractive index changes, providing the mechanism for its electric tuning (as schematically shown in the lower panel of Fig. 1). The implemented approach is based on a recently developed fabrication technology for single-crystal atomically smooth ultrathin gold layers, which has already been used for the experimental demonstration of low-loss plasmonic modes and enhanced nonlinear effects [26,46,49].

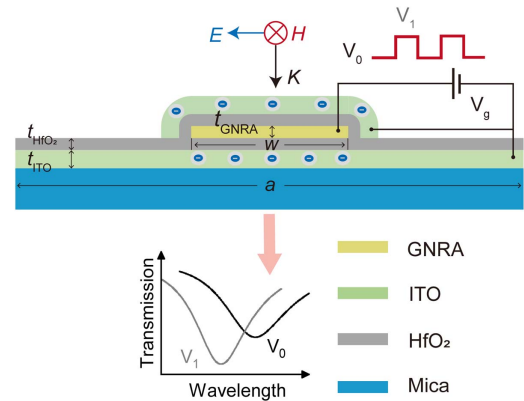


Fig. 1. Schematic illustration of a basic unit of the proposed structure used for electric tuning of plasmonic response in an ultrathin gold nanoribbon array. The thickness, width, and period of the nanoribbons in the array are t_{GNRA} , w , and a , respectively.

First, as a key precursor of the tuning effect, the change in the optical characteristics of ITO in a gold- HfO_2 -ITO structure was investigated under the application of external gate voltages, with the thickness of the HfO_2 layer surrounding the ultrathin GNRA set to a technologically achievable value of 2 nm. Generally, the optical properties of ITO are described by the Drude model [50]. The application of an external bias across the gold- HfO_2 -ITO structure lowers the potential and leads to the accumulation of electrons in the nanoscale ITO region adjacent to the HfO_2 /ITO interfaces. Self-consistent electrostatic simulations reveal that the distribution of the carrier density at the interfaces closely follows an exponential decay function under various applied voltages as shown in Fig. 2(a), presenting an agreement with the Thomas–Fermi approximation [35,51]. Notably, upon the application of a gate voltage as low as 2 V [purple line in Fig. 2(a)], the maximal carrier density is increased by ~ 100 times to the value of $n \sim 10^{27} \text{ m}^{-3}$ at the HfO_2 /ITO boundary, which significantly alters the local plasma frequency $\omega_p^2 = nq^2/\epsilon_0 m^*$ (where $m^* = 0.35m_e$, and q and m_e are the electron charge and mass, respectively). The change of the plasma frequency then drastically modifies the ITO permittivity, $\epsilon_{\text{ITO}} = \epsilon_\infty - \omega_p^2/(\omega^2 + i\omega\gamma)$ (see Appendix A for details), where γ is the electron scattering rate and ϵ_∞ is the high-frequency dielectric constant. As shown in Fig. 2(b), with the increase of the gate voltage from 0 to 2.5 V, at the wavelength of 1.55 μm , the real part of the permittivity of ITO right near the HfO_2 /ITO boundary decreases from a positive value of 3.90 to a negative value of -4.46 , while the corresponding imaginary part increases from essentially 0 to 1.24. Specifically, with the application of a gate voltage of approximately 1.4 V, the ITO can reach a highly attractive epsilon-near-zero (ENZ) regime [marked in Fig. 2(b)] [52]. Overall, due to the exponential decay of the electron density in the ITO near the interface, an ITO layer thickness of 3 nm is large enough for efficient tuning.

3. OPTIMIZATION OF DESIGN

The interaction strength between the plasmonic GNRA and the active ITO layer determines the characteristics of the electric tuning of plasmonic resonance in ultrathin GNRA.

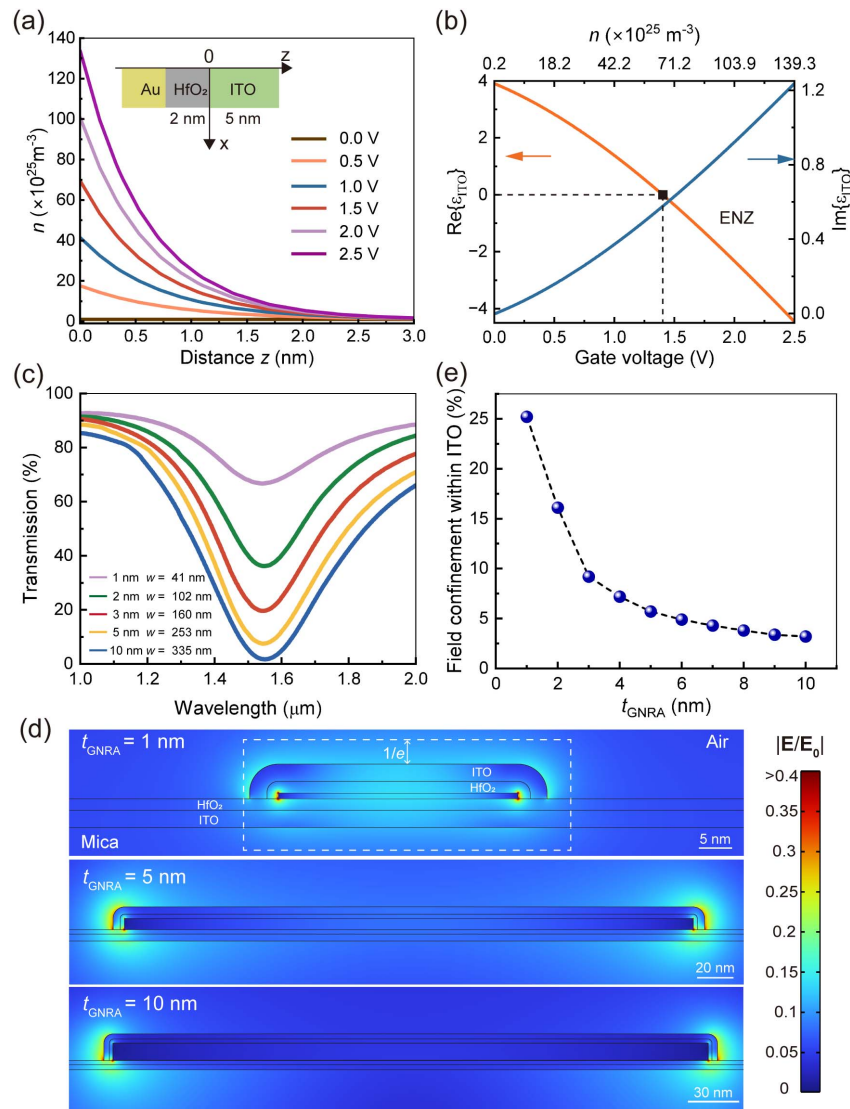


Fig. 2. (a) Numerically calculated electron density inside an ITO layer (initial free electron concentration $n_0 = 10^{25} \text{ m}^{-3}$) in a gold-HfO₂-ITO structure (inset) as a function of the distance from the ITO/HfO₂ interface under the application of various gate voltages. (b) Changes in the optical permittivity of the ITO as a function of the electron density at a wavelength of $1.55 \mu\text{m}$. (c) Simulated transmission spectra (given in percentage of the difference in the transmittances between regions with and without plasmonic structures) of plasmonic structures with various GNRA thicknesses; their peak resonance wavelength is tuned to be the same ($1.55 \mu\text{m}$) by adjusting the nanoribbon width w (see the legend), keeping the period always set to $a = 3w$. (d) Corresponding near-field distributions for active plasmonic structures constructed using GNRA with thicknesses of 1, 5, and 10 nm at the resonance wavelength of $1.55 \mu\text{m}$. (e) Calculated ratios between near-field intensities integrated within the ITO layer and over a rectangular region with the sides separated from the nanoribbon edges by a distance marking $1/e$ electric field decay from the ITO/air interface [see the dashed white box in the top map in (d) as an example] for the plasmonic structures with various GNRA thicknesses.

Therefore, it is important to study the plasmonic properties of the ITO-integrated GNRA (with a 2-nm-thick HfO₂ layer and a 3-nm-thick ITO layer having a free electron concentration of 10^{25} m^{-3}). To carry out accurate electromagnetic simulations, additional optical loss related to the thickness-dependent electron scattering on the ultrathin GNRA boundaries was considered. Particularly, permittivity of single-crystalline gold from Ref. [53] was corrected with the impact of the boundary scattering using the Fuchs theory [54,55] (see Appendix B for details). As shown in Fig. 2(c), to obtain a plasmonic resonance around $1.55 \mu\text{m}$, GNRA with various thicknesses and widths

(keeping the period $a = 3w$) can be used. Specifically, with the gradual decrease in the thickness of the nanoribbons, the required width of the nanoribbons also decreases. The corresponding near-field distributions for plasmonic structures constructed using GNRA with thicknesses of 1, 5, and 10 nm for the resonance wavelength of $1.55 \mu\text{m}$ are presented in Fig. 2(d). One can see that the near-field maps for GNRA with a smaller thickness demonstrate better relative localization of the electromagnetic field in the active ITO region. To quantitatively illustrate this trend, the ratio between near-field intensity integrated within the ITO layer adjacent to the nanoribbon

and the entire integrated near field was calculated [Fig. 2(e)]. The results confirm tighter field confinement and consequently a higher overlap between the mode electromagnetic field and the active ITO layer for smaller nanoribbon thicknesses, which is highly beneficial for greater interaction of the plasmonic mode with the nanoscale permittivity change in ITO to obtain better electric tuning of the plasmonic resonance. Ultrathin GNRA can be fabricated by patterning a large-size ultrathin gold flake into a nanoribbon array using electron-beam lithography and plasma etching techniques as demonstrated in our previous work [26]. Particularly, the thickness of a single-crystal gold flake currently achieved is as small as approximately 2 nm. Therefore, the electric tuning of ITO-integrated GNRA with nanoribbon thickness of 2 nm is first investigated. For the plasmonic resonance in the telecom spectral range, the width of the

nanoribbons for the 2-nm-thick GNRA is determined to be 102 nm [Fig. 2(c)].

4. ELECTRIC TUNING OF PLASMONIC RESONANCE

With the determined optimal parameters of the ITO-integrated ultrathin plasmonic structure, its electric tuning performance was investigated. The transmission spectra of the ITO-integrated ultrathin plasmonic structure having nanoribbons with a thickness $t_{\text{GNRA}} = 2$ nm and a width $w = 102$ nm for various gate voltages are presented in Fig. 3(a). To expose the dependencies in detail, Fig. 3(b) provides a zoomed-in view of the transmission spectra in the wavelength region spanning from 1.45 to 1.6 μm . Then, the values of resonance wavelength

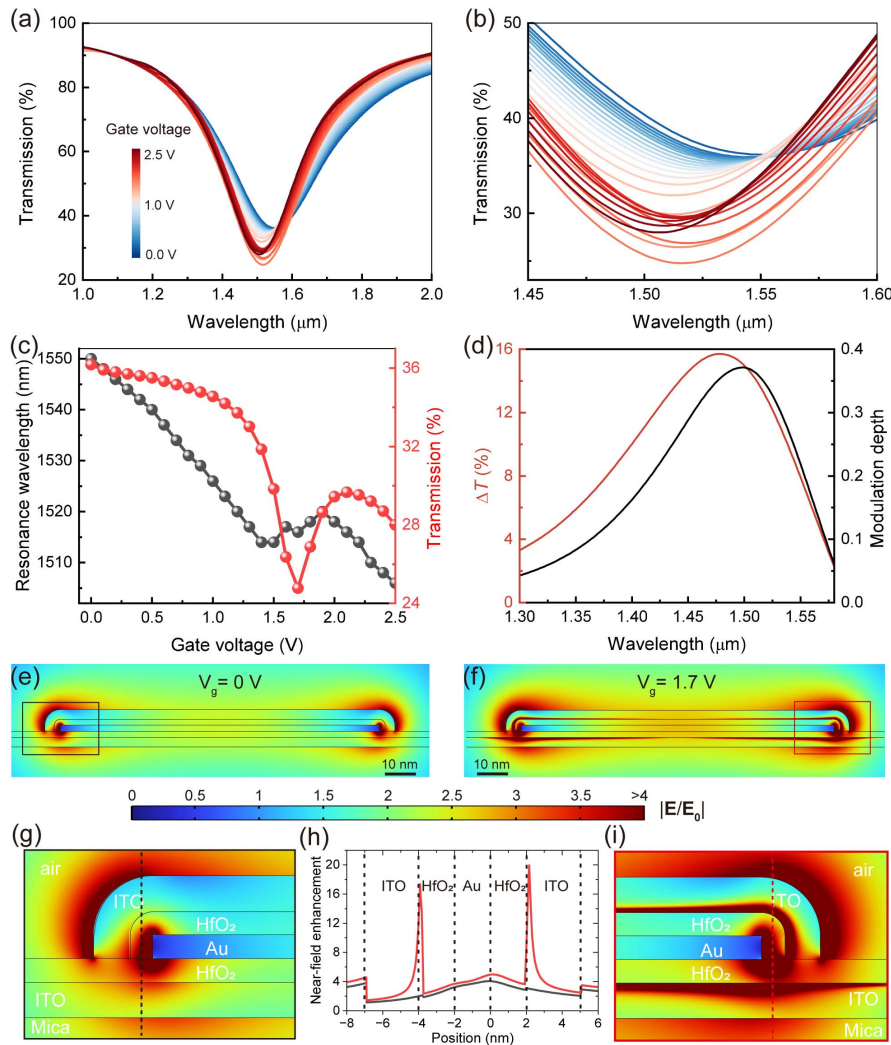


Fig. 3. (a) Dependence of the transmission spectra of the electrically tunable plasmonic design ($t_{\text{GNRA}} = 2$ nm, $w = 102$ nm, $a = 306$ nm, $t_{\text{ITO}} = 3$ nm, and $t_{\text{HfO}_2} = 2$ nm) on the applied gate voltage. (b) Zoomed-in view of (a) in a wavelength range from 1.45 to 1.6 μm . (c) Resonance wavelengths and minimum transmission values for various gate voltages extracted from (b). (d) Variation of the change in the intensity at the transmission dip with the wavelength and corresponding modulation depth upon application of a bias voltage of 1.7 V. (e), (f) Near-field distributions around nanoribbons at the wavelength of 1.55 and 1.516 μm and gate voltages of (e) 0 V and (f) 1.7 V. (g)–(i) Enlarged views (g), (i) of the marked regions in (e) and (f), respectively, together with (h) electric field distribution along the black and red dashed line (1 nm away from the gold edge) in (g) and (i), respectively.

and minimum transmission for various gate voltages are extracted [Fig. 3(c)]. With the rise of the voltage from 0 to 1.4 V, the plasmon resonance dip exhibits a blue-shift for about 36 nm from 1.55 to 1.514 μm , which is due to a gradual decrease in the real part of the permittivity of ITO with an increasing gate voltage. When the voltage increases further, ITO near the HfO_2 interface enters the ENZ regime, which introduces a significant optical loss in the ITO layer due to ENZ-related field enhancement (which will be explained in detail later) and the increase of the imaginary part of ITO permittivity, overall resulting in a rapid decrease of the transmission [Fig. 3(c)]. Particularly, the transmission drops to a minimum value of 24.8% at the bias voltage of 1.7 V. At the same time, the ENZ behavior causes a significant change in the field distribution of the plasmonic mode, which leads to a disruption in the monotonic trends of both characteristics around 1.7 V [Fig. 3(c)]. With a following increase of the voltage from 2.1 to 2.5 V, when the ENZ region moves inside the ITO layer further away from the HfO_2 interface, their behavior is gradually restored to a monotonic decrease. Noting that from the point of view of practical applications, excessively high voltage is more likely to induce the occurrence of tunneling phenomena [35], we restrained the simulated voltages to values below 2.5 V. Overall, the transmission change ($\Delta T = T_{\text{non-gated}} - T_{\text{gated}}$) and the corresponding modulation depth ($1 - T_{\text{gated}}/T_{\text{non-gated}}$) of the ITO-integrated ultrathin plasmonic structure at various wavelengths are shown in Fig. 3(d). One can see that the two characteristics are well correlated. Notably, upon application of a gate voltage of just ~ 1.7 V, the transmission change can lie in the region of 10%–16% in the broad wavelength range from 1.4 to 1.54 μm , with the maximum value of $\sim 16\%$ at the wavelength of 1.47 μm , corresponding to the modulation depth of 0.34. The achieved tunability in resonance wavelength and transmission can be considered to be very substantial as they arise from only a ~ 1 -nm-thick active region in the ITO layer and undoubtedly benefit from the ultraconfined optical field of the nanoribbon plasmonic dipolar resonance. Moreover, to improve the tunability of the plasmonic resonance of the structure, a smaller array period that enhances the density of the nanoribbons together with their coupling can be implemented (see Appendix C for details). At the same time, it is worth noting that the smaller gaps would increase the challenge in device fabrication.

To further elucidate the nature of such electric tuning efficiency, the near-field distributions of the electric field around the nanoribbons at the resonance wavelengths of 1.55 μm and 1.516 μm and gate voltages of 0 and 1.7 V are presented in Figs. 3(e) and 3(f), respectively. The enlarged views of the regions of the field localization shown in Figs. 3(g) and 3(i) demonstrate that under the application of the voltage the optical intensity starts to be confined in the ITO charge accumulation layers. More precisely, the plots of the normalized electric field intensity along the dashed lines in Figs. 3(g) and 3(i) clearly show the pronounced induced electric field in these regions [Fig. 3(h)]. This is related to the increase of the local electric field component normal to the boundary in the ENZ region (present inside the accumulation layer at the applied

voltages above 1.4 V; see Fig. 1) due to the continuity of the corresponding component of the dielectric displacement. Thus, due to the induced field enhancement, the ENZ effect can introduce significant optical loss, which is translated to a rapid decrease of the transmission [Fig. 3(c)]. Therefore, a substantial modulation can be obtained at gate voltages below 1.7 V, which are (1) easily achievable, (2) safe in terms of the dielectric breakdown, and (3) at which tunneling effects can be neglected [35].

The effect of nanoribbon thickness on the electric tuning performance was further investigated. Here, for consistency, the resonance wavelength of the ITO-integrated plasmonic structures with various nanoribbon thicknesses at zero gate voltage is fixed at 1.55 μm by adjusting the nanoribbon widths. Figure 4(a) shows the dependence of the shifts of the plasmonic transmission dips on the gate voltage for ITO-integrated plasmonic structures with various nanoribbon thicknesses. It can be seen that for the same applied gate voltages, the shift of the dip wavelength decreases with the increase of the nanoribbon thickness t_{GNRA} . In addition, Fig. 4(b) shows the corresponding increase in the change of the value of the transmission dip minimum (the corresponding absolute value of the transmission dip is shown in the inset). These results suggest that the tunability of the ITO-integrated nanoribbon array progressively improves with the decrease of the nanoribbon thickness. Specifically, when the thickness of the GNRA is decreased to 1 nm, it gives a spectral shift up to 55 nm and a transmission change of $\sim 13\%$ at a gate voltage of 1.7 V at 1.55 μm . This can be explained by the observation that thinner nanoribbons produce tighter optical field confinement; therefore a much larger portion of plasmonic field interacts with the nanoscale permittivity change in ITO [Fig. 2(e)]. At the same time, for the ITO-integrated nanoribbon arrays constructed using nanoribbons with a thickness of 10 nm and above, the electric tuning effect almost disappears.

The HfO_2 thickness is also a key parameter in determining the self-consistent distributions of the electric potential and the induced carrier density and therefore the distribution of the permittivity change inside the ITO layers. For consistency, the effect of the HfO_2 thickness on the electric tuning performance was investigated by slightly modifying the width of the nanoribbons to keep the same resonance wavelength at 1.55 μm (with the other parameters set as $t_{\text{GNRA}} = 2$ nm, $t_{\text{ITO}} = 3$ nm, and $a = 3w$). As can be seen from Figs. 4(c) and 4(d), the alteration of both the resonance wavelength and the magnitude of the plasmonic transmission dip occurs at smaller applied voltages for smaller thicknesses of HfO_2 . This can be expected, as in this case there is a larger drop in the potential inside the ITO layers, which leads to a higher induced carrier concentration and therefore a more dramatic change in permittivity. In addition, the accompanying smaller overlap between the ultraconfined plasmonic field and the nanoscale electron accumulation layer in the ITO for thicker HfO_2 layers also contributes to the degradation of the electric tunability. Overall, it can be concluded that an ITO-integrated nanoribbon array with smaller nanoribbon and insulator thicknesses has better electric tuning performance. It is worth noting that, for certain applications such as surface-enhanced

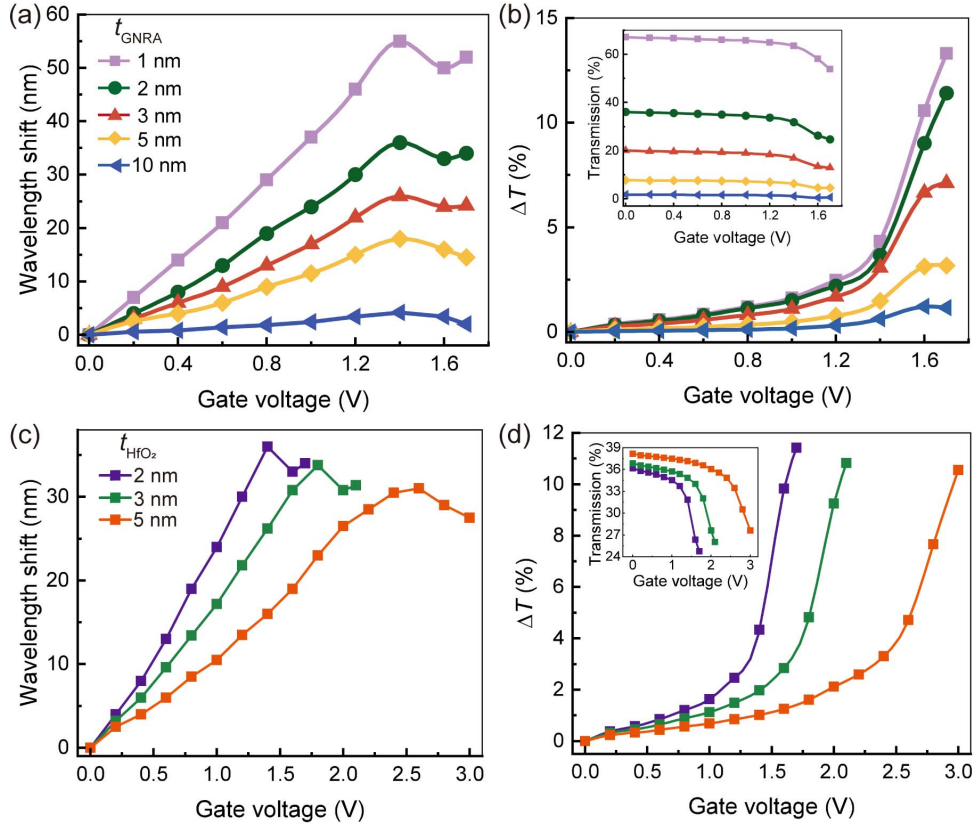


Fig. 4. (a) Dependence of the shift of plasmonic transmission dip on the gate voltage for active plasmonic structure with various nanoribbon thicknesses. (b) Change of the value of the transmission dip as a function of the gate voltage for various nanoribbon thicknesses. Inset: corresponding voltage-dependent absolute values of the magnitude of the transmission dip. (c), (d) Shift of the resonant wavelength as a function of the gate voltage for various HfO_2 thicknesses (c), with the corresponding change of the magnitude of the transmission dip (d). Inset: corresponding voltage-dependent absolute values of the magnitude of the transmission dip.

spectroscopy and spontaneous emission enhancement, the direct access to the optical near fields of ultrathin GNRA is required. Therefore, the electric tunability of 2-nm-thick GNRA with only a bottom ITO layer was also investigated (see Appendix D for details). Under a gate voltage of 1.7 V, a spectral shift of 24 nm and a transmission change of $\sim 10\%$ can be obtained at the wavelength of 1.49 μm .

5. CONCLUSION

In conclusion, by leveraging the resonant extreme light confinement capability of the ultrathin nanoribbons and a dramatic electro-optical effect in ITO, having a particular synergy in the proposed ultrathin design, we have demonstrated an electrically induced 36 nm spectral shift in the plasmonic resonance along with $\sim 16\%$ change in the transmission for a 2-nm-thick GNRA. The operation speed of this electrically tunable plasmonic structure is estimated to be at approximately 2 GHz, as determined by the RC time of the structure (with a device size of $2 \mu\text{m} \times 2 \mu\text{m}$, a gate capacitance of ~ 0.3 pF, and a realistic contact and wiring resistance of ~ 2 k Ω). Being ultrathin and all-solid-state, the proposed electrically tunable ultrathin plasmonic structure is prospective for various applications such as surface-enhanced spectroscopy, spontaneous emission enhancement, and optical modulation.

APPENDIX A: OPTICAL PROPERTIES OF ITO

The permittivity of ITO is defined by the Drude model [35]:

$$\varepsilon_{\text{ITO}}(x, y) = \varepsilon_{\infty} - \frac{\omega_p(x, y)^2}{\omega^2 + i\gamma\omega}, \quad (\text{A1})$$

where $\varepsilon_{\infty} = 3.9$ is the high-frequency dielectric constant and $\gamma = 1.8 \times 10^{14}$ rad/s is the ITO electron relaxation frequency. The local plasma frequency in the carrier accumulation layer,

$$\omega_p(x, y) = \left(\frac{n(x, y)q^2}{\varepsilon_0 m^*} \right)^{\frac{1}{2}}, \quad (\text{A2})$$

is defined by the local electron density $n(x, y)$, which in its term is inter-related with the local potential $\varphi(x, y)$:

$$n(x, y) = \frac{8}{3\sqrt{\pi}} \left(\frac{2\pi m^* q(E_F + \varphi(x, y))}{\hbar^2} \right)^{\frac{3}{2}}, \quad (\text{A3})$$

where

$$E_F = \frac{(3\pi^2 n_0)^{2/3} \hbar^2}{2m^*} \quad (\text{A4})$$

is the ITO Fermi energy and n_0 is the bulk free carrier density in ITO, both at a zero bias; $m^* = 0.35m_e$ is the effective electron mass in ITO, and q is the elementary charge. Under the application of various external biases, the distributions of

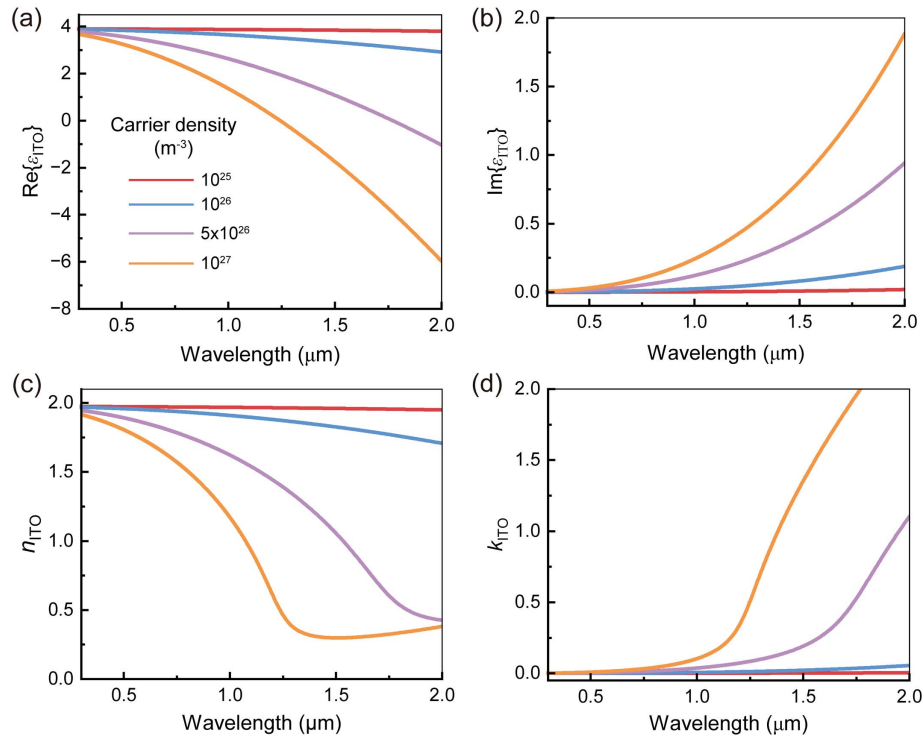


Fig. 5. Permittivity values derived from the Drude model for ITO for various carrier densities. Panels (a) and (b) present the real and imaginary parts of the permittivity, respectively, while panels (c) and (d) show the corresponding real and imaginary parts of the ITO refractive index.

$n(x, y)$ and $\varphi(x, y)$ at the HfO_2/ITO interface were calculated in self-consistent electrostatic numerical simulations. The results were consequently converted to the spatially dependent distribution of ITO permittivity using Eqs. (A1) and (A2). The calculated permittivities and refractive indices of ITO for various carrier densities are presented in Fig. 5.

APPENDIX B: NUMERICAL SIMULATION

The electromagnetic and electrostatic numerical simulations were performed using a finite element method (COMSOL Multiphysics software). As illustrated in the upper panel of Fig. 1, the nanoribbons were illuminated by a normally incident plane wave with its polarization direction perpendicular to the nanoribbons. Given the invariance of the numerical problem along the nanoribbon direction, it is reduced to a two-dimensional case. Taking advantage of the symmetry of the model, a unit cell was simulated with periodic boundary conditions applied to its sides. Additionally, periodic ports were defined to generate the incident plane electromagnetic wave and assure the absence of back-reflection. The array of nanoribbons with a rectangular cross section was modeled; it was characterized by a set of geometrical parameters, nanoribbon width w , thickness t_{GNRA} , and period $a = 3w$ (Fig. 1). The refractive indices of HfO_2 and mica (a standard substrate for ultrathin single-crystal gold flakes, which are precursors for the GNRA) were taken as 1.73 and 1.53, respectively. The static dielectric permittivities of HfO_2 and ITO were taken as 26.2 and 9.3, respectively. Considering the ultrathin nature of the nanoribbons, thickness-dependent electron scattering at

the nanoribbon boundaries was taken into account. Adapting the Fuchs theory [54], permittivity of single-crystal gold from Olmon *et al.* [53] was modified to contain the electron scattering rate including boundary-assisted scattering:

$$\varepsilon_{\text{scf}} = \varepsilon_{\text{Olmon}} + \frac{\omega_p^2}{\omega^2 + i\omega\gamma_{\text{sc}}} - \frac{\omega_p^2}{\omega^2 + i\omega\gamma_{\text{scf}}}, \quad (\text{B1})$$

where $\gamma_{\text{sc}} = 1/\tau_{\text{sc}}$ is the bulk-metal electron relaxation rate, $\tau_{\text{sc}} = 14$ fs is the bulk electron relaxation time, and $\omega_p = 1.231 \times 10^{16}$ Hz is the plasma frequency fit by Olmon *et al.* for a single-crystal case. Here, from the measured permittivity of single-crystal gold, the Drude contribution was subtracted to find the interband permittivity component, and then a modified Drude contribution was added with the scattering rate including the scattering on the boundaries:

$$\gamma_{\text{scf}} = \frac{\gamma_{\text{sc}}}{1 - \frac{3\tau_{\text{sc}}v_F}{2h}(1-p) \int_1^\infty \left(\frac{1}{t^3} - \frac{1}{t^5}\right) \frac{1 - \exp\left(-\frac{h}{\tau_{\text{sc}}v_F t}\right)}{1 - p \exp\left(-\frac{h}{\tau_{\text{sc}}v_F t}\right)} dt}, \quad (\text{B2})$$

where h is the nanoribbon thickness, $p = 0.5$ is the boundary reflection coefficient derived from the experimental observations in Ref. [24], and $v_F = 1.4 \times 10^6$ m/s is the electron Fermi velocity in gold. Using Eqs. (B1) and (B2), modified dielectric function of the nanoribbons was calculated; it is plotted for various nanoribbon thicknesses in Fig. 6. Moreover, one can note that the classical treatment of the optical properties of the ultrathin GNRA using the Drude model is adequate as the plasmonic electron oscillations excited by the normally incident light happen predominantly in the in-plane direction [25,26].

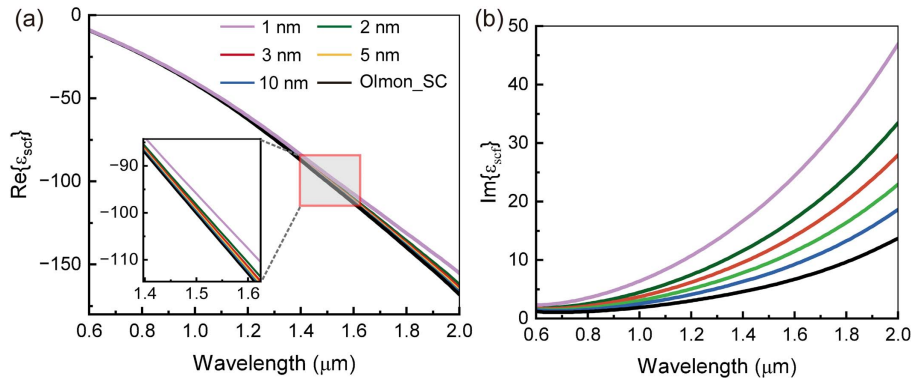


Fig. 6. (a) Real and (b) imaginary parts of the thickness-corrected permittivity of gold for various nanoribbon thicknesses.

APPENDIX C: STRUCTURE WITH A SMALLER ARRAY PERIOD

To further improve the tunability of plasmonic resonance of the structures, arrays with smaller periods (therefore smaller gaps between the nanoribbons), providing more pronounced transmission minima, can be implemented. As shown in Fig. 7, a 20-nm distance between nanoribbons (the width of nanoribbon is adjusted to be 60 nm to maintain the resonance wavelength around 1.55 μm) allows us to achieve twice large modulation depth and resonant wavelength shift (0.86 and 66 nm, respectively, compared with 0.37 and 36 nm previously). This behavior is related

to a combination of a higher density of the resonantly excited nanoribbons per unit length and increased coupling between them due to smaller gaps.

APPENDIX D: STRUCTURE WITH A SINGLE LAYER OF ITO

The top ITO layer in our structure can be removed [Fig. 8(a)], allowing direct access to the near-field of GNRA. As shown in Fig. 8(b), under a gate voltage of 1.7 V, a spectral shift of 24 nm and a transmission change of $\sim 10\%$ (corresponding to a modulation depth of 0.25) can be obtained at the wavelength of 1.49 μm .

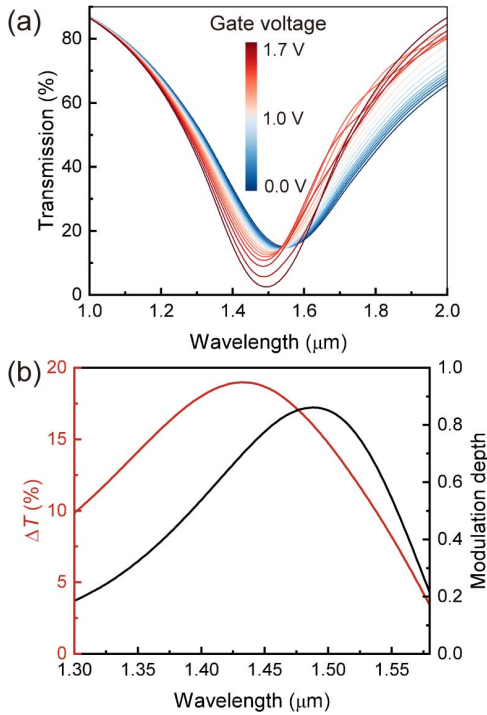


Fig. 7. (a) Transmission spectra of an active plasmonic structure with smaller period and width under different gate voltages ($t_{\text{GNRA}} = 2 \text{ nm}$, $w = 60 \text{ nm}$, $a = 80 \text{ nm}$, $t_{\text{ITO}} = 3 \text{ nm}$, and $t_{\text{HfO}_2} = 2 \text{ nm}$). (b) Variation of the change in the intensity at the transmission dip with the wavelength and corresponding modulation depth.

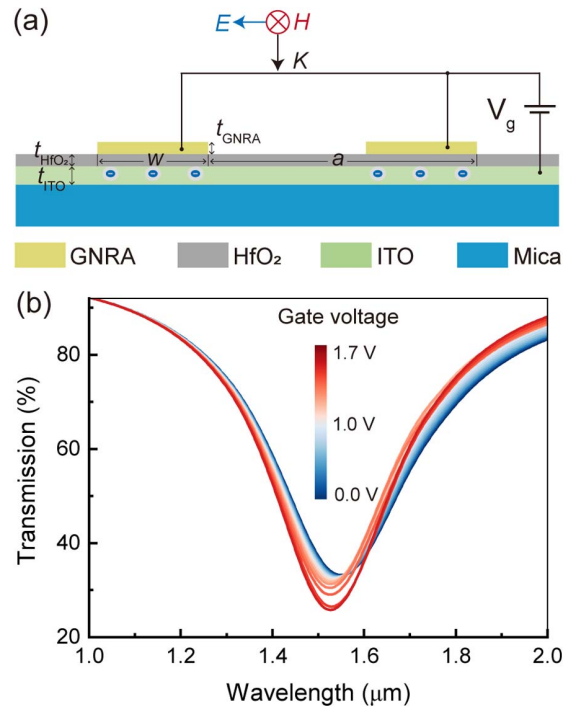


Fig. 8. (a) Schematic of an active plasmonic structure with only a bottom ITO layer used for electric tuning. (b) Corresponding transmission spectra of the active plasmonic structure under different gate voltages ($t_{\text{GNRA}} = 2 \text{ nm}$, $w = 118 \text{ nm}$, $a = 354 \text{ nm}$, $t_{\text{ITO}} = 3 \text{ nm}$, and $t_{\text{HfO}_2} = 2 \text{ nm}$).

Funding. National Natural Science Foundation of China (62075195, 92250305); National Key Research and Development Program of China (2023YFB2806700); The UK EPSRC CPLAS project (EP/W017075/1); Natural Science Foundation of Zhejiang Province (LDT23F04015F05); Fundamental Research Funds for the Central Universities (2023QZJH13).

Disclosures. The authors declare no conflicts of interest.

Data Availability. Data underlying the results presented in this paper are not publicly available at this time but may be obtained from the authors upon reasonable request.

REFERENCES

- D. K. Gramotnev and S. I. Bozhevolnyi, "Plasmonics beyond the diffraction limit," *Nat. Photonics* **4**, 83–91 (2010).
- J. A. Schuller, E. S. Barnard, W. Cai, *et al.*, "Plasmonics for extreme light concentration and manipulation," *Nat. Mater.* **9**, 193–204 (2010).
- H. Xu, E. J. Bjerneld, M. Käll, *et al.*, "Spectroscopy of single hemoglobin molecules by surface enhanced Raman scattering," *Phys. Rev. Lett.* **83**, 4357–4360 (1999).
- E. Ozbay, "Plasmonics: Merging photonics and electronics at nanoscale dimensions," *Science* **311**, 189–193 (2006).
- C. Ciraci, R. T. Hill, J. J. Mock, *et al.*, "Probing the ultimate limits of plasmonic enhancement," *Science* **337**, 1072–1074 (2012).
- M. Kauranen and A. Zayats, "Nonlinear plasmonics," *Nat. Photonics* **6**, 737–748 (2012).
- R. Chikkaraddy, B. de Nijs, F. Benz, *et al.*, "Single-molecule strong coupling at room temperature in plasmonic nanocavities," *Nature* **535**, 127–130 (2016).
- J. Mitchell, "Small molecule immunosensing using surface plasmon resonance," *Sensors* **10**, 7323–7346 (2010).
- A. V. Krasavin and A. V. Zayats, "Guiding light at the nanoscale: numerical optimization of ultrabroadband metallic wire plasmonic waveguides," *Opt. Lett.* **36**, 3127–3129 (2011).
- W. Cai, A. P. Vasudev, and M. L. Brongersma, "Electrically controlled nonlinear generation of light with plasmonics," *Science* **333**, 1720–1723 (2011).
- A. G. Brolo, "Plasmonics for future biosensors," *Nat. Photonics* **6**, 709–713 (2012).
- D. Rodrigo, O. Limaj, D. Janner, *et al.*, "Mid-infrared plasmonic biosensing with graphene," *Science* **349**, 165–168 (2015).
- A. Olivieri, C. Chen, S. A. Hassan, *et al.*, "Plasmonic nanostructured metal–oxide–semiconductor reflection modulators," *Nano Lett.* **15**, 2304–2311 (2015).
- A. V. Krasavin and A. V. Zayats, "Benchmarking system-level performance of passive and active plasmonic components: integrated circuit approach," *Proc. IEEE* **104**, 2338–2348 (2016).
- R. Sokhoyan, P. Thureja, J. Sisler, *et al.*, "Electrically tunable conducting oxide metasurfaces for high power applications," *Nanophotonics* **12**, 239–253 (2023).
- N. Zhou, Y. Yang, X. Guo, *et al.*, "Strong mode coupling-enabled hybrid photon-plasmon laser with a microfiber-coupled nanorod," *Sci. Adv.* **8**, eabn2026 (2022).
- P. Wang, A. V. Krasavin, M. E. Nasir, *et al.*, "Reactive tunnel junctions in electrically driven plasmonic nanorod metamaterials," *Nat. Nanotechnol.* **13**, 159–164 (2018).
- Y.-W. Huang, H. W. H. Lee, R. Sokhoyan, *et al.*, "Gate-tunable conducting oxide metasurfaces," *Nano Lett.* **16**, 5319–5325 (2016).
- F. Moresco, M. Rocca, T. Hildebrandt, *et al.*, "Plasmon confinement in ultrathin continuous Ag films," *Phys. Rev. Lett.* **83**, 2238–2241 (1999).
- E. P. Rugeramigabo, C. Tegenkamp, H. Pfnür, *et al.*, "One-dimensional plasmons in ultrathin metallic silicide wires of finite width," *Phys. Rev. B* **81**, 165407 (2010).
- R. A. Maniyara, D. Rodrigo, R. Yu, *et al.*, "Tunable plasmons in ultrathin metal films," *Nat. Photonics* **13**, 328–333 (2019).
- Z. M. Abd El-Fattah, V. Mkhitarian, J. Brede, *et al.*, "Plasmonics in atomically thin crystalline silver films," *ACS Nano* **13**, 7771–7779 (2019).
- H. Qian, Y. Xiao, and Z. Liu, "Giant Kerr response of ultrathin gold films from quantum size effect," *Nat. Commun.* **7**, 13153 (2016).
- R. Yu, V. Prunerí, and F. J. García de Abajo, "Active modulation of visible light with graphene-loaded ultrathin metal plasmonic antennas," *Sci. Rep.* **6**, 32144 (2016).
- V. Mkhitarian, A. P. Weber, S. Abdullah, *et al.*, "Ultraconfined plasmons in atomically thin crystalline silver nanostructures," *Adv. Mater.* **36**, 2302520 (2023).
- C. Pan, Y. Tong, H. Qian, *et al.*, "Large area single crystal gold of single nanometer thickness for nanophotonics," *Nat. Commun.* **15**, 2840 (2024).
- A. Kossov, V. Merk, D. Simakov, *et al.*, "Optical and structural properties of ultra-thin gold films," *Adv. Opt. Mater.* **3**, 71–77 (2015).
- D. Martínez-Cercós, B. Paulillo, R. A. Maniyara, *et al.*, "Ultrathin metals on a transparent seed and application to infrared reflectors," *ACS Appl. Mater. Interfaces* **13**, 46990–46997 (2021).
- N. Jiang, X. Zhuo, and J. Wang, "Active plasmonics: principles, structures, and applications," *Chem. Rev.* **118**, 3054–3099 (2018).
- L. Zhou, X. Chen, G. Ren, *et al.*, "Electrically tunable SERS based on plasmonic gold nanorod-graphene/ion-gel hybrid structure with a low voltage," *Carbon* **187**, 425–431 (2022).
- Y. Muniz, A. Manjavacas, C. Farina, *et al.*, "Two-photon spontaneous emission in atomically thin plasmonic nanostructures," *Phys. Rev. Lett.* **125**, 033601 (2020).
- I. V. Bondarev, "Controlling single-photon emission with ultrathin transdimensional plasmonic films," *Annalen der Physik* **535**, 2200331 (2023).
- N. K. Emani, T.-F. Chung, A. V. Kildishev, *et al.*, "Electrical modulation of Fano resonance in plasmonic nanostructures using graphene," *Nano Lett.* **14**, 78–82 (2014).
- C. Damgaard-Carstensen and S. I. Bozhevolnyi, "Nonlocal electro-optic metasurfaces for free-space light modulation," *Nanophotonics* **12**, 2953–2962 (2023).
- A. V. Krasavin and A. V. Zayats, "Photonic signal processing on electronic scales: electro-optical field-effect nanoplasmonic modulator," *Phys. Rev. Lett.* **109**, 053901 (2012).
- G. K. Shirmanesh, R. Sokhoyan, P. C. Wu, *et al.*, "Electro-optically tunable multifunctional metasurfaces," *ACS Nano* **14**, 6912–6920 (2020).
- P. Mulvaney, J. Pérez-Juste, M. Giersig, *et al.*, "Drastic surface plasmon mode shifts in gold nanorods due to electron charging," *Plasmonics* **1**, 61–66 (2006).
- J. Wu, A. Y. Bykov, A. V. Krasavin, *et al.*, "Thermal control of polarization of light with nonlocal plasmonic anisotropic metamaterials," *Appl. Phys. Lett.* **123**, 171701 (2023).
- A. N. Koya, J. Cunha, K. A. Guerrero-Becerra, *et al.*, "Plasmo-mechanical systems: principles and applications," *Adv. Funct. Mater.* **31**, 2103706 (2021).
- A. Karki, G. Cincotti, S. Chen, *et al.*, "Electrical tuning of plasmonic conducting polymer nanoantennas," *Adv. Mater.* **34**, 2107172 (2022).
- A. Y. Bykov, Y. Xie, A. V. Krasavin, *et al.*, "Broadband transient response and wavelength-tunable photoacoustics in plasmonic hetero-nanoparticles," *Nano Lett.* **23**, 2786–2791 (2023).
- H. W. Lee, G. Papadakis, S. P. Burgos, *et al.*, "Nanoscale conducting oxide plasmostor," *Nano Lett.* **14**, 6463–6468 (2014).
- J. A. Dionne, K. Diest, L. A. Sweatlock, *et al.*, "Plasmostor: a metal–oxide–Si field effect plasmonic modulator," *Nano Lett.* **9**, 897–902 (2009).
- V. J. Sorger, N. D. Lanzillotti-Kimura, R.-M. Ma, *et al.*, "Ultra-compact silicon nanophotonic modulator with broadband response," *Nanophotonics* **1**, 17–22 (2012).
- G. Kafaie Shirmanesh, R. Sokhoyan, R. A. Pala, *et al.*, "Dual-gated active metasurface at 1550 nm with wide (>300°) phase tunability," *Nano Lett.* **18**, 2957–2963 (2018).
- L. Liu, A. V. Krasavin, J. Zheng, *et al.*, "Atomically smooth single-crystalline platform for low-loss plasmonic nanocavities," *Nano Lett.* **22**, 1786–1794 (2022).

47. C. O. Karaman, A. Y. Bykov, F. Kiani, *et al.*, "Ultrafast hot-carrier dynamics in ultrathin monocrystalline gold," *Nat. Commun.* **15**, 703 (2024).
48. E. Feigenbaum, K. Diest, and H. A. Atwater, "Unity-order index change in transparent conducting oxides at visible frequencies," *Nano Lett.* **10**, 2111–2116 (2010).
49. Z. Wang, L. Liu, D. Zhang, *et al.*, "Effect of mirror quality on optical response of nanoparticle-on-mirror plasmonic nanocavities," *Adv. Opt. Mater.* **11**, 2201914 (2023).
50. R. Amin, R. Maiti, Y. Gui, *et al.*, "Heterogeneously integrated ITO plasmonic Mach-Zehnder interferometric modulator on SOI," *Sci. Rep.* **11**, 1287 (2021).
51. A. Melikyan, N. Lindenmann, S. Walheim, *et al.*, "Surface plasmon polariton absorption modulator," *Opt. Express* **19**, 8855–8869 (2011).
52. J. H. Ni, W. L. Sarney, A. C. Leff, *et al.*, "Property variation in wavelength-thick epsilon-near-zero ITO metafilm for near IR photonic devices," *Sci. Rep.* **10**, 713 (2020).
53. R. L. Olmon, B. Slovick, T. W. Johnson, *et al.*, "Optical dielectric function of gold," *Phys. Rev. B* **86**, 235147 (2012).
54. K. Fuchs, "The conductivity of thin metallic films according to the electron theory of metals," *Math. Proc. Cambridge* **34**, 100–108 (1938).
55. E. H. Sondheimer, "The mean free path of electrons in metals," *Adv. Phys.* **50**, 499–537 (2001).